Ballast with siderurgic aggregates: variation analysis of the shape parameters of particles submitted to triaxial tests through 3D scanner

Maelckson Bruno Barros Gomes[1#] (ID), Antônio Carlos Rodrigues Guimarães[2] (ID),

Filipe Almeida Corrêa do Nascimento[2] (ID), Juliana Tanabe Assad dos Santos[1] (ID)

Article

Abstract

Across countries, associations and institutions publish technical standards for railway ballast, however it is observed that those norms have differences when compared to each other. Each one of them has its particularity, varying according to the stone materials available in their countries, axle load and climate. In that sense, it is still a challenge to establish specific guidelines for the properties of the ballast layer. Recently, several techniques for acquisition, image analysis and particle scanning have been developed, either in 2D or in 3D. Those techniques vary from the use of pachymeter to the use of sophisticated scanners. This research seeks to evaluate, through laboratory tests, the evolution of the particle shape parameters through 3D scanning and the level of degradation of the steel slag when subjected to stresses close to those experienced in freight transport railways. Based on the performed tests and the obtained results, the authors recommend for a railway pavement subjected to a load of 32.5 t/axle and composed of steel aggregates used as ballast, a granulometric distribution with uniformity coefficient $1.5 \leq Cu \leq 1.6$ (AREMA n. 4) and particles with: $0.625 \leq$ Elongation ≤ 0.999, $0.567 \leq$ Flatness ≤ 0.995, $0.475 \leq$ Aspect ≤ 0.969 and $0.825 \leq$ Ellipsoidness ≤ 0.957. These specifications enable a good performance of the ballast layer. In addition, the results found contribute to the understanding of siderurgic aggregate behavior under cyclic loading conditions.

1. Introduction

Over the past decades, there have been numerous researches aiming a better understanding of railway pavements, as well as the performance of their layer materials. The accurate understanding of this subject makes it possible to predict, locate and correct pathologies, avoiding accelerated deterioration and premature failures that may even lead to the interruption of railroad operation (Indraratna & Ngo, 2018).

Rail ballast is the pavement component with the highest weight and volume. It can be found in different granulometries, generally composed of medium and large particles. This layer material usually consists of crushed rocks that vary according to the region where the railway is located. The main used lithologies are: limestone, gneiss, basalt, quartzite, granite, rhyolite, dolomite, etc (Selig & Waters, 1994; Raymond & Diyaljee, 1994).

In this context, and aiming the reuse of materials, steel slag has been widely studied, particularly in geotechnical works and in transport infrastructure. Steel slag is a by-product resulting from the steel manufacturing process. It has been observed that, after adequate processing, chemical and environmental stabilization, this material can be an excellent alternative to natural aggregates especially when it can be found close to the pavement to be built (Fernandes, 2010; Delgado et al., 2019; Chamling et al., 2020; Guimarães et al., 2021; Indraratna et al, 2022;).

In 2020, 622 kg of waste/co-products were generated per ton of steel produced in Brazil, of which approximately 25% resulted in steel slag. That means 155 kg of steel slag for each ton of steel produced (Brazilian Steel Institute, 2020). According to the Worldsteel Association (2022), around 31 million tons of steel were produced in Brazil that year. Therefore, approximately 19.3 million of waste/co-products and 4.8 million tons of steel slag were generated in 2020. This high availability associated with the current increase in demand for rail network expansion show a window of opportunity to combine economic growth with sustainability.

Numerous associations and institutions in different countries publish technical standards guiding the use of materials in the ballast layer. It is observed that the technical standards for railway ballast have differences when compared to each other. Each one of them has its particularity, varying according to the stone materials available in their countries, axle load and climate.

For example, the Brazilian standard for rail ballast NBR 5564/2011 (ABNT, 2021) was limited to tests to be carried out with particles or a set of particles, but not mentioning their lithologies. On the other hand, the same standard republished in October 2021, brings the limits to be observed according to the lithology, however, it does not mention the steel aggregates, which can be seen in the American standard.

It is still difficult to establish strict constitutive standards and models for the properties of the ballast layer (Fortunato, 2005). However, it is known that the layer behavior is essentially conditioned by its mechanical (strength and deformability) and hydraulic (permeability) characteristics.

Thus, it is desirable that these values remain relatively constant throughout the passage of railway compositions and the lifetime of the track. Nevertheless, the stability of this rate is hampered by the gradual increase in long-term stiffness of the material when cyclically loaded. This phenomenon can be intensified if the particles used in the layer have a propensity to produce fines when subjected to the imposed forces.

Although there is still no consensus on the standards to be followed in the world, with regard to the execution of the ballast layer, the parameters that define its behavior are:
- the characteristics of the individual particles: size, shape, texture, angularity, lithology, weathering level, mineralogical composition, durability, hardness, specific weight and toughness;
- the characteristics of the particles set: granulometric curve, void ratio, thickness of the ballast layer and degree of saturation; and
- loading characteristics: main stress, confining pressure, the ratio between the main stress and the confining pressure, stress history, current stress state, number of cycles, frequency and amplitude.

While the properties of individual particles interfere in their degradation under cyclic traffic loading, deformation is also influenced by magnitude, frequency, stress ratio and the number of load cycles (Indraratna et al., 2011; Sun et al., 2014a, 2016).

Therefore, this research seeks to evaluate, through laboratory tests, the evolution of the particle shape parameters through 3D scanning and the level of degradation of the steel slag when subjected to stresses close to those experienced in freight transport railways. The results found contribute to the understanding of steel aggregate behavior under cyclic loading conditions.

1.1 Triaxial tests

The elastic-plastic behavior of the material used in railway ballast is traditionally investigated through laboratory tests, either to obtain its resilient modulus or to predict its plastic deformation under a certain number of cycles. For laboratory studies of railway ballasts, the greatest difficulty found is to reproduce a ballast layer with its real granulometry, with some particles with dimensions equal to or greater than 63.5 mm, preventing the use of triaxial equipment of traditional dimensions (100 x 200 mm and 150 x 300 mm).

In order to overcome this problem, several authors have been using two alternatives: scaling the granulometric curve and large-scale triaxial equipment. Alabbasi & Hussein (2019) presents a summary of the dimensions of the specimen compatible with triaxial equipment and the relation between the diameter of the specimen and the maximum diameter of the particles (D/d_{max}) established. It is observed that both the size of the specimens and the relation D/d_{max} are not a consensus among the different authors.

In Brazil, the national standard for determining permanent deformation, DNIT 179/2018 (DNIT, 2018) guides that in case of granular material, the ratio between the maximum particle diameter and the specimen diameter must be 1:4. Furthermore, if the sample shows material retained in the 1" sieve but completely passing through the 1.1/2" sieve, a cylinder with a 150 mm diameter and 300 mm height must be used. Therefore, these were the ratio and the sample used in this research.

When testing a granular material with a high number of cyclic loadings, one of the most important parameters is the development and accommodation of the plastic deformations. This phenomenon is described by the shakedown theory, proposed for paving materials analysis by Werkmeister et al. (2001). Figure 1 illustrates typical responses of soils and granular aggregates subjected to cyclic loading.

During stage A, known as plastic shakedown, the material accumulates plasticity during several load applications, until deformations increment is practically zero, which results in a final behavior considered purely elastic. During stage B, called plastic creep, high levels of plastic deformation rate, which the material shows in the first load cycles, decrease rapidly until they reach a relatively low and approximate constant value.

The transition from stage A to stage B is normally related to a rapid increase in resilient deformations. For higher stress states, the material behavior goes to stage C, called incremental collapse, where successive increases in plasticization occur. In this case, the rate of plastic deformation either decreases very slowly, or does not decrease at all. It also can lead to rupture.

Werkmeister et al. (2001) suggests that the best way to investigate the occurrence of shakedown is to plot the permanent deformation curves according to the criterion expressed by Dawson and Wellner model (Dawson & Wellner,
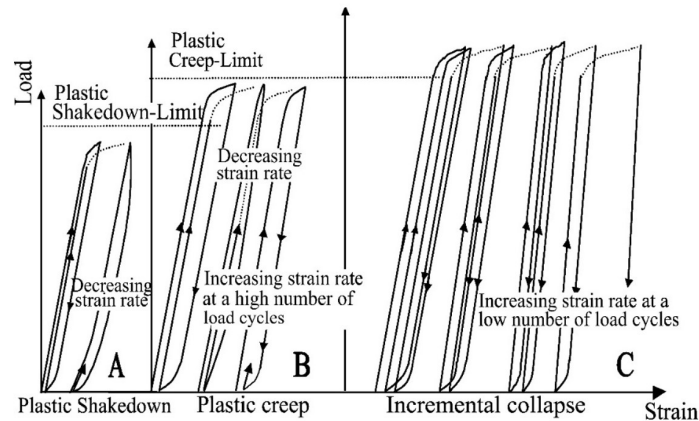
Figure 1. Typical responses of soils and granular aggregates subjected to cyclic loading (Werkmeister et al. (2001).

1999). These authors found that materials with adequate long-term behavior tend to stabilize permanent deformations when their rate of increase at each load application cycle was of the order of 10⁻⁷ mm/load cycle.

During repeated load tests, it is possible to measure the material resilient modulus (*RM*) through ratio between σ_d and ε_r (where σ_d is the difference between maximum and minimum stresses, and ε_r is the recoverable axial strain during triaxial cyclic load) under the same cyclic stress state. Guimarães (2009) observes that, for stages A and B, the resilient deformation is relatively constant throughout the load application cycles, and its magnitude varies according to the type of material and the state of stress applied. However, for stage C, if the material begins to show granulometric evolution (considerable morphological changes of the particles), a drop in *RM* will be evidenced, which should stabilize again for the new granulometric distribution, however, at a new level of magnitude.

1.2 Particle scanning

Recently, several techniques for acquisition, image analysis and particle scanning have been developed, either in 2D or in 3D. Each one of them with its own particularity, ranging from the use of pachymeter to the use of sophisticated scanners. Three particle analysis scales are traditionally established: shape, angularity and texture (Figure 2). Shape is a larger scale feature; texture is a microscopic feature and angularity is an intermediate scale feature.

Regarding the shape, which is the focus of this research, most quantifications are based on the measurement of the longest (*L*), shortest (*S*) and intermediate (*I*) orthogonal dimensions, being commonly combined two by two: elongation (*I/L*), flattening (*S/I*) and aspect ratio (*S/L*). The elongation and flattening parameters vary between 0 and 1 and seek to demonstrate how close the particles are to being planar, columnar, spherical or planar-columnar, according to the classification proposed by Zingg (1935). After the Zingg
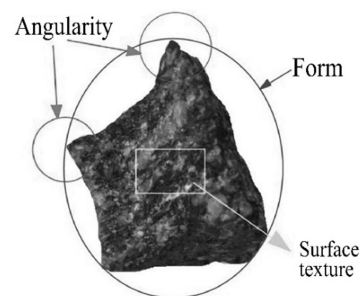

Figure 2. Shape characteristics of a ballast particle (Guo et al., 2019).

diagram, many researchers proposed new diagrams and modifications to the existing ones (Graham & Gadsden, 2019), such as proposed by Blott & Pye (2008).

3D analysis provides a more realistic analysis of the particle, considering the possible distortions that a 2D or 2.5D analysis can generate. In addition, the correct assessment of particle degradation can be compromised if the particles break instead of only being polished by abrasion (Fonseca et al., 2012; Guo et al., 2019).
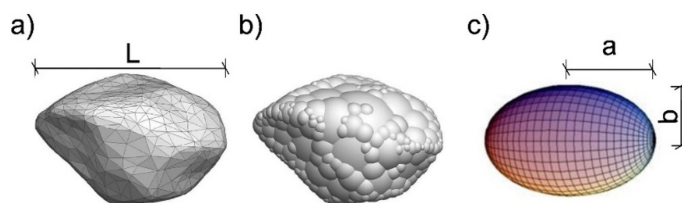
Considering this, (Sun et al., 2014a) proposed an alternative to quantify the shape of particles with 3D scanning called "ellipsesity". This factor represents how closely the analyzed particle approaches the shape of an ellipsoid and it is defined as the division of the surface area of an ellipsoid of the same volume as the particle, and the actual surface area of the particle. The factor varies between 0 and 1, meaning that the closer the ellipses of the particle is to 1, the more it resembles an ellipsoid of prolate revolution, which is an ellipsoid that has a larger radius (*a*) and two equal radii (*b* =*c*<*a*), smaller.

According to Table 1, the parameters established to obtain the ellipsoidness ratio are:

The ellipsoid surface area is twice the area generated by rotating the first-quadrant portion of the ellipse (Equation 1) about the x-axis, resulting in Equation 2, which entails in

Table 1. Ellipsoidness ratio parameters (Gomes et al., 2022).

Equation	Where
$a=\dfrac{L}{2}$	a = Ellipsoid largest radius; and L = Longest particle length (Figure 3a).
$b=c=\sqrt{\dfrac{3V}{2\pi L}}$	b = c<a for a prolate ellipsoid (Figure 3c); b and c = Equal and smaller radii of the ellipsoid; and V = Particle volume.
$S_e=2\pi\left\{b^2+a^2\cdot\dfrac{\arccos\left(\dfrac{b}{a}\right)}{\tan\left[\arccos\left(\dfrac{b}{a}\right)\right]}\right\}$	Se = Ellipsoid surface area with the same volume as the particle.
$E=\dfrac{S_e}{S_o}$	E = Ellipsoidness; So = Particle surface area

Figure 3. (a) Simulated ballast particle: Scanned surface of a real ballast particle, (b) corresponding virtual particle made of spheres and (c) ellipsoid with the same volume as the ballast particle. Adapted from: Bono et al. (2020).

Equation 3 and after numerical development, generates Equation 4. More details on the development of the ellipsoidness ratio can be seen in Gomes et al. (2022).

$$\frac{x^2}{a^2}+\frac{y^2}{b^2}=1,\ a>b \tag{1}$$

$$s_e=2\int_0^a 2\pi y\sqrt{1+\left(\frac{dy}{dx}\right)^2}\,dx \tag{2}$$

$$1+\left(\frac{dy}{dx}\right)^2=\frac{a^4+b^2x^2-a^2x^2}{a^4-a^2x^2} \tag{3}$$

$$s_e=2\pi\left\{b^2+a^2\frac{\arccos\left(\frac{b}{a}\right)}{\tan\left[\arccos\left(\frac{b}{a}\right)\right]}\right\} \tag{4}$$

1.3 Particles degradation

The understanding of the way particles generates fines, how their morphological characteristics change and the impact on layers deformation has shown to be relevant. It assists the development of increasingly sophisticated numerical models to describe particles set behavior under stress.

Some authors have focused on describing the contact mechanism and the way in which contact degradation occurs. Among them are Bono et al. (2020) and Ngo & Indraratna (2020), who modeled particles to a discrete element model through 3D scanning of real particles (Figure 3a and 3b) in order to increase modelling accuracy.

Although the contact between irregular particles and their interactions when subjected to cyclic stress is still complex, the way particle degradation occurs can be grouped into the following types (Wang et al., 2019; Lees & Kennedy, 1975; Guo et al., 2019): abrasion (surface polishing), fracture (particle breakage generating two or more new smaller particles), friction (sharp edges removal) and chipping (removal of chips from particles).

The occurrence of the events of particle degradation is related to particles size, applied stresses and granulometry. Indraratna et al. (2018) showed, however, that most of the ballast degradation is not related to particles splitting, but mainly to edges breaking.

Regarding the evolution of particle shape parameters before and after laboratory tests, Paixão & Fortunato (2021) investigated the performance of a steel slag submitted to the Micro-Deval test and morphological parameters evolution

4

Gomes et al., Soil. Rocks, São Paulo, 2023 46(3):e2023006122

through a low-cost photogrammetry method and compared to a granite result. It was concluded that the morphological alterations of the slag were smaller and more uniform, despite the fact that the two materials presented similar Micro-Deval abrasion coefficients.

Also, through the Micro-Deval test, Quintanilla et al. (2019) used an X-ray tomography device and identified that in the first revolutions of the test there is a tendency to break the sharp and more angular edges of the particles. Consequently, there is an increase in the contact area at the end of these edges wear. However, it was concluded that the test is not able to change the general shape of the grains, being limited to the surface polishing.

Indraratna et al. (2016) used a 3D laser scanner to obtain the morphological parameters of particles. The materials were molded into cylindrical specimens and subjected to dynamical triaxial tests at frequencies of 20 Hz and 30 Hz. A rise in the ellipsoidness ratio (E) and in the flatness ratio was observed after the tests were carried out. The particles became progressively rounded and regular while the frequency of load application was being increased. In view of the executed tests, a range for the ellipsoidness ratio of the evaluated particles was proposed, with the purpose of attenuating degradation and deformation under high cyclic loading frequencies.

In triaxial tests performed on stony materials, in addition to the deformations quantified through *LVDT*s (Linear Variable Differential Transformer), it is necessary to evaluate particles degradation. Some approaches have been developed in the last few decades, and can be categorized into two main types: particle breaking single-grading indices and global-grading indices (Xiao et al., 2021).

The *Bg* proposed by Marsal (1967) is the particle breaking single-grading indices most used by researchers of railway ballast while *BBI* (Indraratna et al., 2005), *B* (Einav, 2007) and *Br* (Hardin, 1985) are the commonly used particle breaking global-grading indices.

Single-grading indices do not usually represent the breakage of all different sizes particles. On the other hand,

global-grading indices are established by assuming the potential breakage of all particles (Xiao et al., 2021).

2. Material properties and performed tests

2.1 Materials

The material used in this research was a steel slag from the Ternium S.A. steel mill located in the state of Rio de Janeiro, Brazil. The slag was chemically and environmentally inert when it was made available for the development of the studies. Characterization tests were carried out (determination of the particles shape, apparent specific mass, apparent porosity, water absorption, resistance to weathering, mass loss by Los Angeles abrasion and resistance to shock through the Treton equipment) following the Brazilian guidelines, according to standard NBR 5564:2021 (ABNT, 2021) that establishes requirements and test methods for railway ballast.

The results were compared with those found by Delgado (2019), with the limits established in Manual for Railway Engineering of AREMA (2015), standard for steel aggregate, and with the Brazilian standard, ABNT (2021), for other lithologies. Regarding shape, non-cubic particles, apparent specific mass, wear resistance and shock resistance, the slag met the limits to be observed, according to the Table 2.

2.2 Particle scanning proceedings

To investigate the particles morphological parameters variation when submitted to repeated loads triaxial tests, it was delimited the sampling effort of 54 particles. They were selected following AREMA n. 4 particle size distribution (Figure 4), resulting in 18 particles per specimen (6 per sieve interval), randomly selected.

The equipment used to digitize the particles was the portable scanner GO!SCAN 3D from CREAFORM, from the robotics laboratory of the Military Institute of Engineering with linear and volumetric accuracy up to 0.10 mm and 0.30 mm/m

Table 2. Aggregate's properties

Parameter	Value	ABNT (2021) limit	AREMA (2015) limit	Delgado (2019)
		Other lithologies	Steel Slag	Steel Slag
Average particle shape	cubic	cubic	cubic	cubic
Non-cubic particles	7%	<15%	<5%	7%
Apparent specific mass	3.153 kg/m³	>2.500 kg/m³	>2.900 kg/m³	3.200 kg/m³
Water absorption	3.9%	<2.0%	<2.0%	1.7%
Apparent porosity	11.0%	<2.0%	-	-
Wear resistance (Los Angeles abrasion)	10.6%	<30%	<30%	23%
Shock resistance (Treton toughness index)	5.2%	<25%	-	-
Powdery material	0.1%	<1%	<1%	0%
Clay clods	0.0%	<0.50%	<0.50%	-
Unit mass limit in loose state	1585 kg/m³	>1250 kg/m³	-	-

respectively, and resolution up to 0.50 mm. The object digitization was executed through VXScan software and meshes were treated with the VXModel software. Reflective targets were placed on the table used in the digitization in order to better capture light beams emitted by the scanner.

Before being submitted to digitalization, the particles were identified following a pre-defined pattern after performing permanent deformation test. In that way, they were painted in different colors, according to the granulometry, and numbered from 1 to 6, as specified in Table 3 and Figure 5.

Each particle was scanned 3 times (turning each particle 90°) in order to establish common mesh intervals between

successive scans and join the meshes to form the definitive particle. The VXModel allows to fit each particle into a cube, in order to obtain its largest, smallest and intermediate dimensions (Figure 5b).

In addition, it allows the extraction of the surface area as well as the particle volume. The values got from scans were used to obtain the classification according to the Zingg diagram, and to investigate the modifications imposed on the particles by the cyclic tests, as suggested by Indraratna et al. (2016).

2.3 Repeated load triaxial tests

Permanent deformation analysis was carried out through the Repeated Load Triaxial Test (RLTT) results that were executed in a triaxial apparatus similar to that presented in Figure 6. In this test, a state of stress is applied repeatedly to assess the material response to a given number of loading cycles.

Three specimens of around 150 mm of diameter and 300 mm of height were used. The samples were subjected to 250,000 load cycles with cyclic axial loads ($\sigma 1$) on the top at a frequency of 2 Hz and static axisymmetric loads ($\sigma 3$).

The specimens were molded by vibration in four layers with a granulometric distribution according to AREMA n. 4 (Figure 4). It was performed the regularization of the top of the specimens (Figure 7b) with paster before submitting
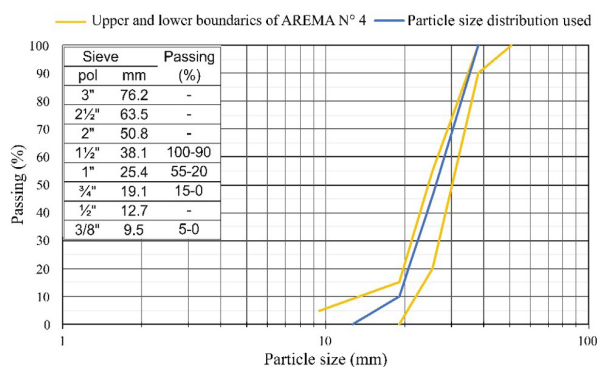

Figure 4. AREMA n. 4 particle size distribution.

Figure 5. (a) Scanning proceedings: Painted particles and reflective targets in place and (b) an example of a scanned particle fitted into a cube.

Table 3. Identifying particles.

Color	Sieve interval	Particle identification
Blue	Particles passing through the 1.1/2" sieve and retained in the sieve 1"	A1, A2, A3, A4, A5 and A6
Green	Particles passing through the 1" sieve and retained in the 3/4" sieve	B1, B2, B3, B4, B5 and B6
Yellow	Particles passing through the 3/4" sieve and retained in the 1/2" sieve	C1, C2, C3, C4, C5 and C6

them through the triaxial apparatus. More details about this procedure can be found on Gomes (2022). As a result of this procedure, the void index (e) and uniformity coefficient (Cu) used were similar to the values found by other authors who performed large-scale triaxial tests, such as Lackenby et al. (2007) and Indraratna et al. (2016).

Scanned particles constituted the two intermediate specimen layers (Figure 7a). The objective of this method is to mitigate possible distortions if they were placed on the top, which is immediately in contact with the place of load application, or at the bottom, where it might not faithfully reproduce the transition between the ballast and subballast layer.

The stress state applied on the test was a main stress of 350 kPa with a confining pressure of 70 kPa and a 280 kPa deviator stress. This state of tension is commonly observed in heavy haul railways and was conducted by Delgado et al. (2021) in a steel aggregate with similar characteristics to this

research. This stress state, conducted at a 2 Hz frequency, reproduces a train formed by GBT-type gondola wagons with a 1.60 m gauge and a 32.5 t/axle load operating at an average speed of 80 km/h.

The conditioning phase was performed with the same stress state of the permanent deformation test, in which the first 500 cycles were considered to simulate the tamping process performed in the execution of railway pavements. This process was adopted at the Soil Laboratory of the Military Engineering Institute (Figure 7c).

After the conditioning phase, the system coupled to the equipment automatically collects data referring to: cycle number, plastic deformation, elastic deformation, plastic displacement, elastic displacement, accumulated elastic displacement and final height of the specimen.

3. Analysis and results

3.1 Permanent deformation and particles breakage

Table 4 present the ballast breakage rates obtained during the permanent deformation tests (CP-01, CP-02 e CP-03). From the evaluation of the other parameters of the material, such as void index (e) and uniformity coefficient (Cu), it was considered that the procedure used for specimens molding proved to be satisfactory.

It is observed that all three specimens had type A behavior (plastic shakedown). The level observed in Figure 8 indicates an almost null plastic deformations increase and a purely elastic response to cyclic loading.

The studies performed allowed the verification of the magnitude of plastic deformations of less than 1.5 mm. Furthermore, the permanent deformations of specimens CP-02 and CP-03 starting from cycle number 150,000 onwards remained practically collinear. The resilient module in the initial cycles were similar, around 400 MPa, indicating a

1 – Workbench;
2 – Triaxial chamber rail;
3 – Reaction gantry;
4 – Triaxial chamber;
5 – Load cell;
6 – Servomotor;
7 – Pressure regulating filter;
8 – Control totem;
9 – Control and monitoring interface;
10 – USB connector;
11 – Reset button;
12 – General power button;
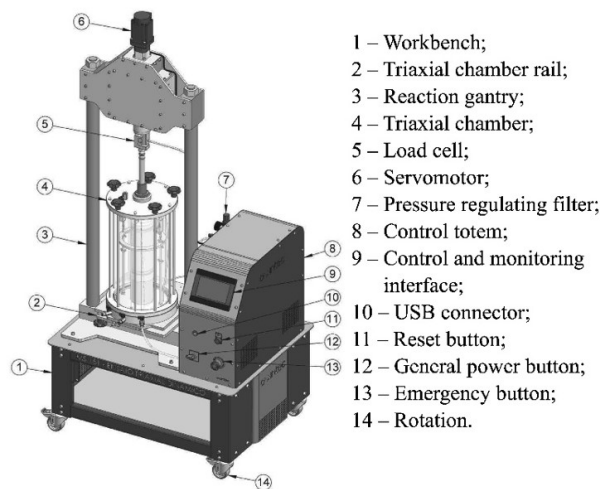13 – Emergency button;
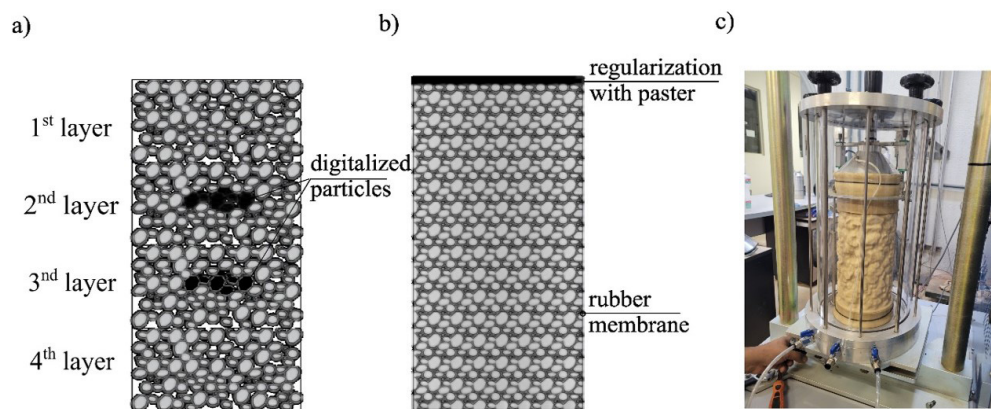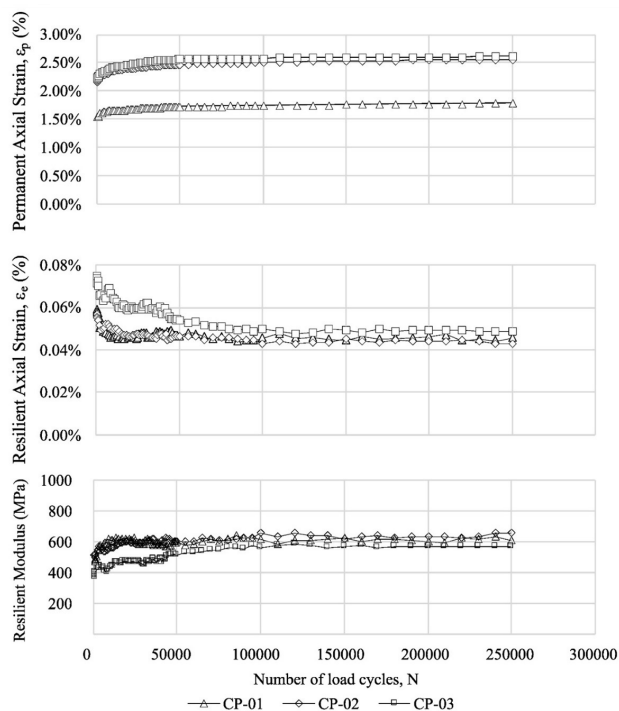14 – Rotation.

Figure 6. Triaxial apparatus.

Figure 7. (a) Scanned particles positioned in layers, (b) specimen after conditioning and top regularization with paster and (c) specimen in triaxial chamber.

Table 4. Ballast breakage rates obtained.

Specimen	e	Cu	σ_1 (kPa)	σ_3 (kPa)	σ_d (kPa)	σ_1/σ_3	Bg (Marsal, 1967)	Br (Hardin, 1985)	BBI (Indraratna et al., 2005)	B (Einav, 2007)
CP-01	0.81	1.50	350	70	280	5	0.031	0.008	0.030	0.015
CP-02	0.74	1.59	350	70	280	5	0.016	0.009	0.036	0.017
CP-03	0.84	1.51	350	70	280	5	0.020	0.012	0.044	0.021

Figure 8. Mechanical parameters: permanent axial strain (ε_r), resilient axial strain (ε_p) and resilient modulus (RM) according to number of load cycles.

Figure 9. Relation between real particle mass and its corresponding scanned volume.
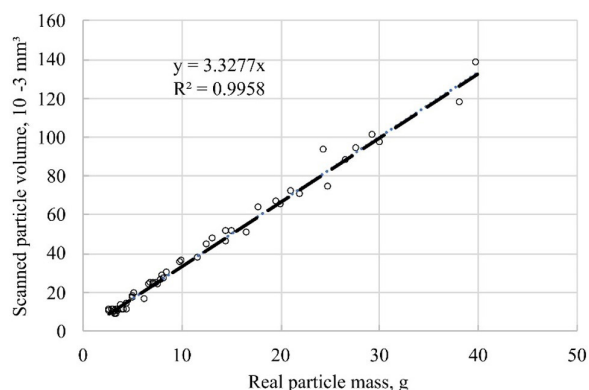
probable repeatability of the procedure imposed in specimens' preparation for the laboratory tests and constancy of the intrinsic parameters of the material.

The breakage potentials vary according to the granulometric distribution. Well-graded grading curves have a low breaking potential compared to uniform grading curves if Br or BBI are to be used. Therefore, the use of different indices must be done with caution to obtain the degradation values of the analyzed granulometric curves.

On the other hand, there is a similar behavior of the B, Br and BBI indices. The Bg index was similar to the other indices only in CP-02 and CP-03. This difference in behavior is reported by Indraratna et al. (2016) who found a different behavior pattern for Bg index when the uniformity coefficient and maximum particle diameter varied in triaxial tests.

3.2 Particle size and shape variation

From the digitization of the 54 particles (18 per specimen) it was possible to obtain morphological parameters, with an accuracy of 0.01mm, of particles with d_{max}=37.5 mm (1.1/2"). In Figure 9 it is possible to verify the scan adherence to the actual particle digitization, since the angular coefficient (3.327) of the linear trend line found was similar to the specific mass of the material 3153.0 kg/m³, after the conversion of the measurement unit.

Through the Zingg diagram it was possible to observe the before and after of the particle's classification. All particles were classified as cuboid which is the recommended shape for a particle that composes ballast layer.

Figure 10 presents graphs with the Zingg diagram classification obtained before and after the permanent deformation tests. Table 5 allows evaluating the variation of the ratios of elongation, flatness, aspect and ellipsoidness of the eighteen known particles in each of the three specimens.

In relation to the ellipsoidness, for the evaluated particles, a minimum value of 0.825 and a maximum value of 0.957 were obtained (Figure 11). It was also not possible to observe a parameter modification pattern regarding to specimen dimensions.

It is noted that with a considerable sampling effort, in tests conducted with tensions, uniformity coefficients, void index and very similar aggregates, the modifications obtained by the particles were variable. This is an indication that the evolution of morphological parameters is still difficult to describe and are related to more intrinsic and extrinsic factors.

Indraratna et al. (2016) observed an increase in the rates of elongation, flatness, aspect and ellipsoidness in a basalt. It was evaluated that the particles suffered surface abrasion or

Table 5. Shape characteristics of scanned particles.

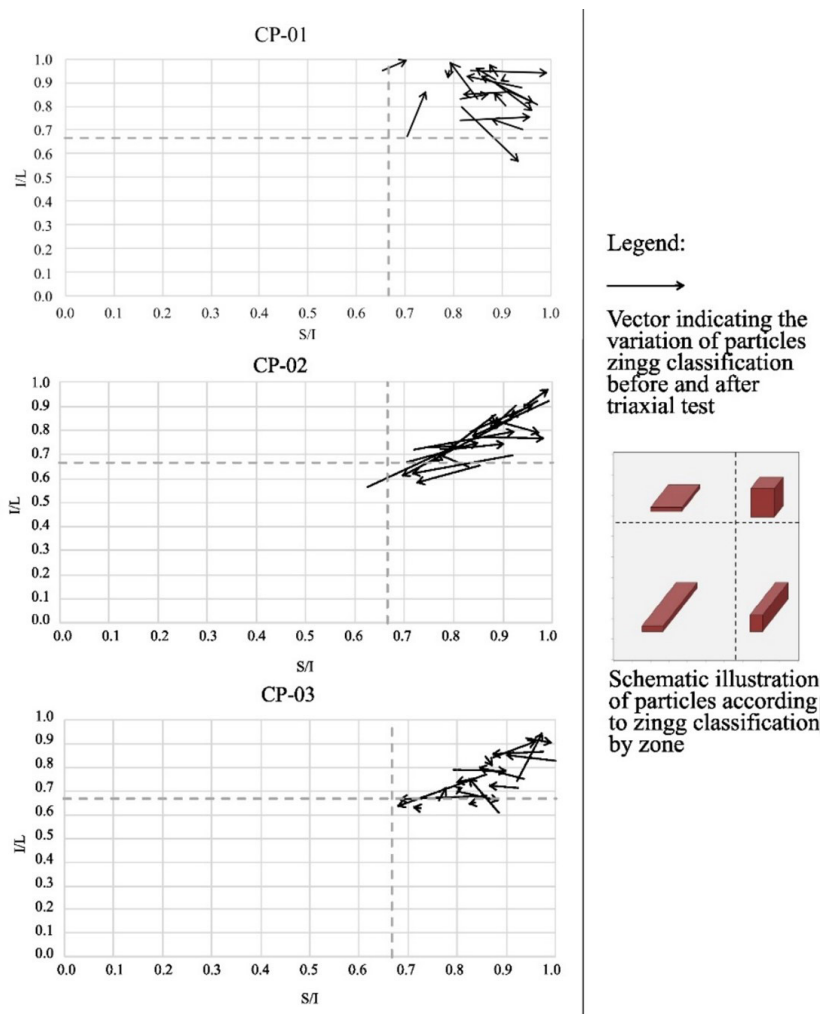| Specimen	Particle	Elongation ratio (*I/L*)		Flatness ratio (*S/I*)		Aspect ratio (*S/L*)		Ellipsoidness	
		before	after	before	after	before	after	before	after
CP-01	A1	0.850	0.794	0.833	0.985	0.708	0.782	0.860	0.866
	A2	0.818	0.932	0.796	0.566	0.651	0.527	0.840	0.843
	A3	0.888	0.961	0.895	0.784	0.795	0.753	0.860	0.860
	A4	0.908	0.884	0.801	0.855	0.727	0.756	0.857	0.874
	A5	0.939	0.828	0.881	0.930	0.827	0.769	0.865	0.873
	A6	0.972	0.859	0.809	0.928	0.787	0.797	0.873	0.877
	B1	0.814	0.956	0.741	0.755	0.603	0.722	0.846	0.836
	B2	0.705	0.743	0.674	0.860	0.475	0.639	0.886	0.870
	B3	0.886	0.847	0.915	0.963	0.810	0.816	0.908	0.926
	B4	0.834	0.991	0.953	0.942	0.795	0.934	0.929	0.929
	B5	0.653	0.703	0.950	0.995	0.621	0.699	0.888	0.883
	B6	0.892	0.876	0.928	0.973	0.827	0.852	0.880	0.888
	C1	0.912	0.963	0.866	0.817	0.789	0.787	0.949	0.957
	C2	0.789	0.788	0.951	0.920	0.750	0.725	0.867	0.868
	C3	0.814	0.870	0.832	0.848	0.677	0.738	0.875	0.908
	C4	0.903	0.898	0.915	0.914	0.826	0.821	0.904	0.907
	C5	0.910	0.821	0.862	0.852	0.784	0.700	0.902	0.918
	C6	0.943	0.880	0.702	0.746	0.662	0.657	0.838	0.876
CP-02	A1	0.994	0.839	0.923	0.778	0.923	0.778	0.827	0.842
	A2	0.880	0.972	0.841	0.791	0.841	0.791	0.877	0.880
	A3	0.706	0.848	0.670	0.750	0.670	0.750	0.888	0.872
	A4	0.969	0.915	0.921	0.856	0.921	0.856	0.888	0.903
	A5	0.835	0.958	0.796	0.902	0.796	0.902	0.906	0.904
	A6	0.927	0.874	0.902	0.806	0.902	0.806	0.874	0.868
	B1	0.886	0.758	0.866	0.671	0.866	0.671	0.909	0.925
	B2	0.852	0.726	0.653	0.586	0.653	0.586	0.849	0.855
	B3	0.720	0.922	0.718	0.795	0.718	0.795	0.850	0.837
	B4	0.784	0.901	0.720	0.743	0.720	0.743	0.849	0.841
	B5	0.625	0.789	0.567	0.719	0.567	0.719	0.889	0.857
	B6	0.918	0.696	0.849	0.613	0.849	0.613	0.890	0.919
	C1	0.829	0.769	0.650	0.702	0.650	0.702	0.900	0.901
	C2	0.748	0.805	0.733	0.734	0.733	0.734	0.925	0.935
	C3	0.941	0.992	0.898	0.969	0.898	0.969	0.874	0.877
	C4	0.879	0.886	0.862	0.822	0.862	0.822	0.947	0.939
	C5	0.863	0.981	0.774	0.770	0.774	0.770	0.894	0.895
	C6	0.920	0.717	0.697	0.624	0.697	0.624	0.877	0.927
CP-03	A1	0.925	0.867	0.712	0.723	0.712	0.723	0.847	0.845
	A2	0.884	0.825	0.608	0.751	0.608	0.751	0.860	0.872
	A3	0.941	0.990	0.925	0.904	0.925	0.904	0.842	0.835
	A4	0.874	0.957	0.841	0.912	0.841	0.912	0.880	0.888
	A5	0.799	0.882	0.697	0.661	0.697	0.661	0.825	0.828
	A6	0.999	0.901	0.827	0.852	0.827	0.852	0.890	0.910
	B1	0.859	0.684	0.680	0.667	0.680	0.667	0.881	0.894
	B2	0.762	0.778	0.661	0.712	0.661	0.712	0.875	0.872
	B3	0.860	0.681	0.771	0.639	0.771	0.639	0.875	0.859
	B4	0.842	0.800	0.758	0.739	0.758	0.739	0.886	0.903
	B5	0.935	0.845	0.750	0.801	0.750	0.801	0.854	0.849
	B6	0.973	0.873	0.868	0.858	0.868	0.858	0.898	0.913
	C1	0.727	0.711	0.628	0.634	0.628	0.634	0.879	0.893
	C2	0.793	0.898	0.791	0.785	0.791	0.785	0.896	0.884
	C3	0.835	0.826	0.650	0.647	0.650	0.647	0.946	0.946
	C4	0.858	0.871	0.847	0.811	0.847	0.811	0.878	0.861
	C5	0.922	0.972	0.743	0.942	0.743	0.942	0.890	0.894
	C6	0.802	0.808	0.708	0.713	0.708	0.713	0.897	0.895

Figure 10. Evolution of particles shapes parameters submitted to triaxial test.
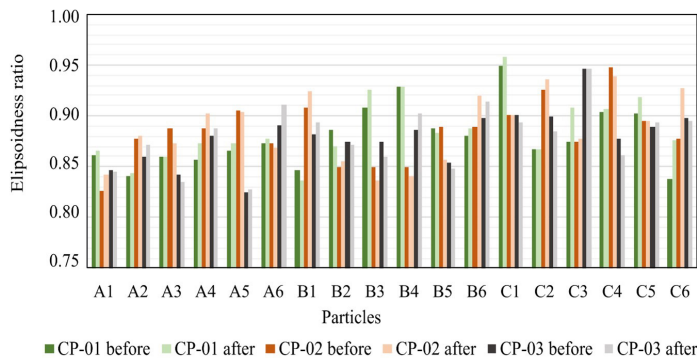

Figure 11. Elipsoidness ratio variation of particles.

chipping with a tendency to become closer to a cube. However, it is noteworthy that the digitized particles of the present research, despite not having presented a pattern of evolution of the morphological parameters, were already predominantly cubic before the tests and remained that way after the tests.

According to Indraratna et al. (2018), for a ballast to have good mechanical performance, it is recommended that the ellipsoidness ratio of the particles be in a range of 0.375 to 0.376. This interval should probably be revised, or, at least, not generalized to all cases, according to the results

found here. This can contribute to the selection of materials for the ballast layer in a more assertive way.

4. Conclusions

The rail ballast behavior under high tensions imposed by heavy loads is an investigation that interests many researchers. Its correct understanding can inhibit possible degradations that may compromise the integrity of the railway pavement in service during the project lifetime.

In this work, a method of scanning the particles through a portable 3D scanner was presented. This study proved to be promising in view of the current scientific interest in computationally simulating physical phenomena (Alabbasi & Hussein, 2021).

Digitization made it possible to classify the particles based on the dimensions obtained with an accuracy of 0.01mm. However, it was not possible to observe a trend of shape parameters evolution for the steel aggregate.

For this reason, further triaxial testing is recommended. This methodology, along with the box test, is composed of tests that describe the behavior of the in-situ layer more faithfully than the Los Angeles and Micro-Deval abrasion tests.

The steel aggregate showed low plastic deformations for the imposed stress state. The values were similar to those found by Delgado et al. (2021), who conducted tests with the same stress state of this research in a steel aggregate in Portugal.

The breakage indices obtained were similar to those found by other authors (Sun et al., 2014b; Indraratna et al., 2016; Delgado et al., 2021; Sun & Zheng, 2017). After the tests, ruptured particles were not identified (i.e. particles giving rise to two or more new particles), but only surface polishing and breaking of sharp corners, which is an indication that the particles have a high crushing resistance.

Finally, based on the performed tests and the obtained results, the authors recommend for a railway pavement subjected to a load of 32.5 t/axle and composed of steel aggregates used as ballast, a granulometric distribution with $1.5 \leq Cu \leq 1.6$ (AREMA n. 4) and particles with: $0.625 \leq$ Elongation ≤ 0.999, $0.567 \leq$ Flatness ≤ 0.995, $0.475 \leq$ Aspect ≤ 0.969 and $0.825 \leq$ Ellipsoidness ≤ 0.957. Therefore, a good behavior of the material regarding permanent deformations and draining characteristics is expected, considering the low level of fines generated after 250,000 loading cycles.

This recommendation of values for the ellipsoidness ratio disagrees with what was recommended by Indraratna et al. (2016, 2018), which suggests a very small range, ranging from $0.375 \leq$ ellipsoidness ≤ 0.376. Although Indraratna et al. (2016) have recommended this range of ellipsoidness ratio based on high frequency tests, it is believed that this value should be reviewed or, at least, not applied to all scenarios of: loading, frequency, lithology and particle size distribution.

Declaration of interest

The authors declare that they have no known competing financial interests or personal relationships that could have appeared to influence the work reported in this paper.

Authors' contributions

Maelckson Bruno Barros Gomes: writing- original draft preparation, data curation, methodology, investigation. Antônio Carlos Rodrigues Guimarães: validation, supervision. Filipe Almeida Corrêa do Nascimento: visualization, supervision. Juliana Tanabe Assad dos Santos: writing - review & editing.

Data availability

The raw and processed data required to reproduce these findings are available to download from: https://drive.google.com/drive/folders/1OAWW1uoztAX0n5uYj-WXrcJMXuV4-md9?usp=sharing

List of symbols

a	Major axis
b, c	Minor radii
e	Void index
B	Breakage index proposed by Einav (2007)
BBI	Ballast breakage index proposed by Indraratna et al. (2005)
Bg	Breakage index proposed by Marsal (1967)
Br	Breakage index proposed by Hardin (1985)
Cu	Uniformity coefficient
D	Specimens diameter
D_{10}	Particle diameters defining 10% finer from the grain-size distribution curve
D_{60}	Particle diameters defining 60% finer from the grain-size distribution curve
d_{max}	Maximum diameter of particles
E	*E*llipsoidness ratio
I	Intermediate dimension
L	Longest dimension
PD	Permanent Deformation
RM	Resilient Modulus
S_o	Real surface
S_e	Surface area of an ellipsoid having the same volume as the scanned particle
S	Shortest dimension

Gomes et al., Soil. Rocks, São Paulo, 2023 46(3):e2023006122

11

V	Volume of the scanned particle
V_v	Volume of voids
V_s	Volume of solids
ε_r	Elastic strain
σ_d	Deviator stress
σ_l	Maximum major stress
$\sigma_{lmax,cyclic}$	Maximum cyclic major stress
σ_3	Minimum major stress or confining pressure

References

ABNT NBR 5564. (2021). *Railroad - rail ballast - requirements and test method*. ABNT - Associação Brasileira de Normas Técnicas, Rio de Janeiro, RJ (in Portuguese).

Alabbasi, Y., & Hussein, M. (2019). Large-scale triaxial and box testing on railroad ballast: a review. *SN Applied Sciences*, 1, 1592. https://doi.org/10.1007/s42452-019-1459-3.

Alabbasi, Y., & Hussein, M. (2021). Geomechanical modelling of railroad ballast: a review. *Archives of Computational Methods in Engineering*, 28, 815-839. http://dx.doi.org/10.1007/s11831-019-09390-4.

American Railway Engineering Maintenance-of-way Association - AREMA. (2015). *Manual for railway engineering* (Vol. 1-4). AREMA.

Blott, S.J., & Pye, K. (2008). Particle shape: a review and new methods of characterization and classification. *Sedimentology*, 55, 31-63. http://dx.doi.org/10.1111/j.1365-3091.2007.00892.x.

Bono, J., Li, H., & McDowell, G. (2020). A new abrasive wear model for railway ballast. *Soil and Foundation*, 60(3), http://dx.doi.org/10.1016/j.sandf.2020.05.001.

Brazilian Steel Institute. (2020). *Three foundations of sustainable development*. Retrieved in April 2, 2022, from https://www.acobrasil.org.br/relatoriodesustentabilidade/#ambiental

Chamling, K., Haldar, S., & Patra, S. (2020). Physico-chemical and mechanical characterization of steel slag as Railway Ballast. *Indian Geotech J*, 50(2), 267-275. http://dx.doi.org/10.1007/s40098-020-00421-7.

Dawson, A.R., & Wellner, F. (1999). *Plastic behaviour of granular materials* (Final Report ARC Project, 933). Department of Civil Engineering, University of Nottingham.

Delgado, B., Da Fonseca, A., Fortunato, E., & Motta, L. (2019). *Aproveitamento de escórias de aciaria em infraestruturas de transportes - estudos e aplicações em Portugal e no Brasil*. Retrieved in April 14, 2022, from http://repositorio.lnec.pt:8080/jspui/handle/123456789/1012121

Delgado, B.G. (2019). *Geomechanics of an inert steel aggregate as an alternative material for heavy haul railway ballast* [Doctoral thesis, Faculty of Engineering]. University of Porto (in Portuguese). Retrieved in April 14, 2022, from https://hdl.handle.net/10216/125559

Delgado, B.G., Fonseca, A.V., Fortunato, E., Paixão, A., & Alves, R. (2021). Geomechanical assessment of an inert steel slag aggregate as an alternative ballast material for heavy haul rail tracks. *Construction & Building Materials*, 279, http://dx.doi.org/10.1016/j.conbuildmat.2021.122438.

DNIT 179/2018–IE. (2018). *Paving – Soils – Determination of Permanent Deformation – Test Instruction*. DNIT - Departamento Nacional de Infraestrutura de Transportes. Rio de Janeiro, RJ. (in Portuguese).

Einav, I. (2007). Breakage mechanics—Part I: theory. *Journal of the Mechanics and Physics of Solids*, 55(6), 1274-1297. http://dx.doi.org/10.1016/j.jmps.2006.11.003.

Fernandes, D.P. (2010). *Study of chemical, geo-mechanical and environmental stabilization of LD steel slag for application as railway ballast material on signalized roads* [Master thesis]. Ouro Preto Federal University. (in Portuguese). Retrieved in April 2, 2022, from http://www.repositorio.ufop.br/bitstream/123456789/2325/1/DISSERTA%c3%87%c3%83O_EstudoEstabiliza%c3%a7%c3%a3oQu%c3%admica.pdf

Fonseca, J., O'Sullivan, C., Coop, M.R., & Lee, P. (2012). Non-invasive characterization of particle morphology of natural sands. *Soil and Foundation*, 52, 712-722. http://dx.doi.org/10.1016/j.sandf.2012.07.011.

Fortunato, E. (2005). *Renewal of railway platforms: studies on load capacity* [Doctoral dissertation, LNEC/Engineering College] Porto University (in Portuguese). Retrieved in April 14, 2022, from https://hdl.handle.net/10216/11441

Gomes, M., Guimarães, A., & Nascimento, F. (2022). Revisão do cálculo do parâmetro para quantificar tridimensionalmente a morfologia das partículas de lastro: a elipsoidade. In *Anais Eletrônicos do 36° Congresso de Pesquisa e Ensino em Transportes*. Fortaleza, Ceará. (in Portuguese). Retrieved in December 21, 2022, from https://proceedings.science/anpet-2022/trabalhos/revisao-do-calculo-do-parametro-para-quantificar-tridimensionalmente-a-morfologi?lang=pt-br#

Gomes, M.B.B. (2022). *Análise da deformabilidade do lastro ferroviário de agregado siderúrgico utilizando ensaios triaxiais de cargas repetidas* [Master Thesis, Transportation Engineering]. Military Institute of Engineering. (in Portuguese). http://dx.doi.org/10.13140/RG.2.2.12223.59048.

Graham, D.J., & Gadsden, R.J. (2019). New statistical methods for the comparison and characterization of particle shape. *Earth Surface Processes and Landforms*, 44, 2396-2407. http://dx.doi.org/10.1002/esp.4669.

Guimarães, A.C.R. (2009). *An empirical mechanistic method for the prediction of permanent deformation in tropical soils constituent of pavements* [Doctor thesis, Civil Engineering Program]. Federal University of Rio de Janeiro (in Portuguese). Retrieved in April 2, 2022, from http://www.coc.ufrj.br/pt/teses-de-doutorado/153-2009/1199-antonio-carlos-rodrigues-guimaraes

Guimarães, A.C.R., Costa, K.Á., Reis, M.M., Santana, C.S.A., & Castro, C.D. (2021). Study of controlled leaching process of steel slag in soxhlet extractor aiming employment in pavements. *Transportation Geotechnics*, 27, http://dx.doi.org/10.1016/j.trgeo.2020.100485.

Guo, Y., Markine, V.L., Zhang, X., Qiang, W., & Jing, G. (2019). Image analysis for morphology. rheology and degradation study of railway ballast. *Transportation Geotechnics*, 18, 173-211. http://dx.doi.org/10.1016/j.trgeo.2018.12.001.

Hardin, B. O. (1985). Crushing of soil particles. *Journal of Geotechnical Engineering*, 111(10), 1177-1192. https://doi.org/10.1061/(ASCE)0733-9410(1985)111:10(1177).

Indraratna, B., & Ngo, T. (2018). *Ballast railroad design: smart-uow approach*. CRC Press. https://doi.org/10.1201/9780429504242.

Indraratna, B., Lackenby, J., & Christie, D. (2005). Effect of confining pressure on the degradation of ballast under cyclic loading. *Geotechnique*, 55(4), 325-328. http://dx.doi.org/10.1680/geot.2005.55.4.325.

Indraratna, B., Ngo, N.T., Nimbalkar, S., & Rujikiatkamjorn, C. (2018). Two decades of advancement in process simulation testing of ballast strength, deformation, and degradation. In T.D. Stark, R.H. Swan & R. Szecsy (Eds.), *Railroad ballast testing and properties* (pp. 11-38). West Conshohocken, United States: ASTM International. http://dx.doi.org/10.1520/STP160520170029.

Indraratna, B., Qi, Y., Tawk, M.H.A., Rujikiatkamjorn, C., & Navaratnarajah, S.K. (2022). Advances in ground improvement using waste materials for transportation infrastructure. *Proceedings of the Institution of Civil Engineers: Ground Improvement*, 175(1), 3-22. http://dx.doi.org/10.1680/jgrim.20.00007.

Indraratna, B., Salim, W., & Rujikiatkamjorn, C. (2011). *Advanced rail geotechnology – ballasted track*. CRC Press. https://doi.org/10.1201/b10861.

Indraratna, B., Sun, Y., & Nimbalkar, S. (2016). Laboratory assessment of the role of particle size distribution on the deformation and degradation of ballast under cyclic loading. *Journal of Geotechnical and Geoenvironmental Engineering*, 142(7), http://dx.doi.org/10.1061/(ASCE)GT.1943-5606.0001463.

Lackenby, J., Indraratna, B., McDowell, G., & Christie, D. (2007). Effect of confining pressure on ballast degradation and deformation under cyclic triaxial loading. *Géotechnique*, 57(6), 527-536. https://doi.org/10.1680/geot.2007.57.6.527.

Lees, G., & Kennedy, C.K. (1975). Quality, shape and degradation of aggregates. *Quarterly Journal of Engineering Geology and Hydrogeology*, 8(3), 193-209. http://dx.doi.org/10.1144/GSL.QJEG.1975.008.03.03.

Marsal, R.J. (1967). Large scale testing of rockfill materials. *Journal of the Soil Mechanics and Foundations Division*, 93(2), 27-43. http://dx.doi.org/10.1061/JSFEAQ.0000958.

Ngo, T., & Indraratna, B. (2020). Analysis of deformation and degradation of fouled ballast: experimental testing and DEM modeling. *International Journal of Geomechanics*, 20, 06020020. http://dx.doi.org/10.1061/(ASCE)GM.1943-5622.0001783.

Paixão, A., & Fortunato, E. (2021). Abrasion evolution of steel furnace slag aggregate for railway ballast: 3D morphology analysis of scanned particles by close-range photogrammetry. *Construction & Building Materials*, 267, http://dx.doi.org/10.1016/j.conbuildmat.2020.121225.

Quintanilla, I.D., Combe, G., Emeriault, F., Voivret, C., & Ferellec, J. (2019). X-ray CT analysis of the evolution of ballast grain morphology along a Micro-Deval test: key role of the asperity scale. *Granular Matter*, 21, http://dx.doi.org/10.1007/s10035-019-0881-y.

Raymond, G. P., & Diyaljee, V. A., (1994). Railroad ballast sizing and grading. *Journal of the Geotechnical Engineering Divison*, 105(5), 676-681. https://doi.org/10.1061/AJGEB6.0000803.

Selig, E.T., & Waters, J.M. (1994). *Track geotechnology and substructure management*. Thomas Telford. https://doi.org/10.1680/tgasm.20139.0007.

Sun, Y., Indraratna, B., & Nimbalkar, S. (2014a). Three-dimensional characterisation of particle size and shape for ballast. *Géotechnique Letters*, 4(3), 197-202. http://dx.doi.org/10.1680/geolett.14.00036.

Sun, Q.D., Indraratna, B., & Nimbalkar, S. (2014b). Effect of cyclic loading frequency on the permanent deformation and degradation of railway ballast. *Geotechnique*, 64(9), 746-751. http://dx.doi.org/10.1680/geot.14.T.015.

Sun, Q.D., Indraratna, B., & Nimbalkar, S. (2016). The deformation and degradation mechanisms of railway ballast under high frequency cyclic loading. *Journal of Geotechnical and Geoenvironmental Engineering*, 142(1). 04012056. https://doi.org/10.1061/(ASCE)GT.1943-5606.0001.

Sun, Y., & Zheng, C. (2017). Breakage and shape analysis of ballast aggregates with different size distributions. *Particuology*, 35, 84-92. http://dx.doi.org/10.1016/j.partic.2017.02.004.

Wang, Y., Shao, S., & Wang, Z. (2019). Effect of particle breakage and shape on the mechanical behaviors of granular materials. *Advances in Civil Engineering*, 2019, 1-15. http://dx.doi.org/10.1155/2019/7248427.

Werkmeister, S., Dawson, A.R., & Wellner, F. (2001). Permanent deformation behavior of granular materials and the shakedown concept. *Transportation Research Record: Journal of the Transportation Research Board*, 1757(1), 75-81. http://dx.doi.org/10.3141/1757-09.

Worldsteel Association. (2022). *Global crude steel output decreases by 0.9% in 2020*. Retrieved in April 7, 2022, from https://worldsteel.org/media-centre/press-releases/2021/global-crude-steel-output-decreases-by-0-9-in-2020/

Xiao, Y., Wang, C., Wu, H., & Desai, C.S. (2021). New simple breakage index for crushable granular soils. *International Journal of Geomechanics*, 21(8), 04021136. http://dx.doi.org/10.1061/(ASCE)GM.1943-5622.0002091.

Zingg, T. (1935). Beitrag zur schotteranalyse. *Schweizerische Mineralogische und Petrographische Mitteilungen*, 15, 39-140. http://dx.doi.org/10.3929/ethz-a-000103455.